The Viral protein Corona Directs Viral Pathogenesis and Amyloid Aggregation

Kariem Ezzat[1], Maria Pernemalm[2], Sandra Pålsson[3], Thomas C. Roberts[4,5], Peter Järver[3], Aleksandra Dondalska[3], Burcu Bestas[1], Michal J. Sobkowiak[6], Bettina Levänen[7], Magnus Sköld[7,8], Elizabeth A. Thompson[9], Matthew J.A. Wood[4], Ultan F. Power[10], Sergej Masich[11], Anders Lindén[7], Johan K. Sandberg[6], Janne Lehtiö[2], Anna-Lena Spetz[3]*, Samir EL Andaloussi[1,4]*

[1]Department of Laboratory Medicine, Clinical Research Center, Karolinska Institutet, Stockholm, Sweden.

[2]Clinical Proteomics Mass Spectrometry, Department of Oncology-Pathology, Science for Life Laboratory, and Karolinska Institutet, Stockholm, Sweden

[3]Department of Molecular Biosciences, The Wenner-Gren Institute, Stockholm University, Stockholm, Sweden.

[4]Department of Physiology, Anatomy and Genetics, University of Oxford, Oxford, UK.

[5]Sanford Burnham Prebys Medical Discovery Institute, Development, Aging and Regeneration Program, La Jolla, CA, USA.

[6]Center for Infectious Medicine, Department of Medicine, Karolinska Institutet, Karolinska University Hospital Huddinge, Stockholm, Sweden.

[7]Institute of Environmental Medicine (IMM), Karolinska Institutet, Stockholm, Sweden.

[8]Lung Allergy Clinic, New Karolinska Solna, Karolinska University Hospital, Stockholm, Sweden.

[9]Institutionen För Medicin, Karolinska Institutet, Stockholm, Sweden.

[10]Centre of Experimental Medicine, Queens' University Belfast, Belfast, United Kingdom.

[11]Department of Cell and Molecular Biology, Karolinska Institutet, Stockholm, Sweden.

*Equal contribution.

Correspondence should be addressed to KE: kariem.ezzat.ahmed@ki.se and A-LS: anna-lena.spetz@su.se

Abstract

Nanoparticles accumulate a plethora of host factors on their surface (protein corona) in biological fluids, which influence the nanoparticle activity. Here we provide evidence for the existence of a rich viral protein corona and show its implications for viral infectivity, immune cell activation and catalysis of amyloid aggregation. We demonstrate that respiratory syncytial virus (RSV), a major cause of respiratory tract infections, accumulates a distinctive protein corona in different biofluids including: human plasma, human bronchoalveolar lavage fluid, non-human primate plasma and fetal bovine serum. Additionally, corona pre-coating differentially affects viral infectivity and its ability to activate human monocyte-derived dendritic cells (moDCs) depending on the biofluid. Furthermore, we demonstrate that cell-free RSV can bind and catalyze the amyloid aggregation of an amyloidogenic peptide derived from the islet amyloid polypeptide (IAPP) via surface-assisted nucleation. Similarly, we show that herpes simplex virus 1 (HSV-1) catalyzes the amyloid aggregation of the amyloid-beta ($A\beta_{42}$) peptide which is the major constituent of amyloid plaques in Alzheimer's disease. Our results provide a proof-of-concept for the presence of a viral protein corona layer that is dependent on the microenvironment and influences viral-host interactions. Additionally, the demonstration of viral nanosurface driven amyloid catalysis in an extracellular environment illustrates convergence between viral and amyloid pathologies suggesting a novel mechanistic link that warrants further investigation.

Keywords: protein corona, respiratory syncytial virus (RSV), herpes simplex virus 1 (HSV-1), Alzheimer's disease, amyloid

Significance

Outside cells, viruses are biophysically equivalent to synthetic nanoparticles as they rely on intracellular machinery for replication. Here we show that similar to nanoparticles, viruses accumulate a rich and unique layer of host factors in different biological fluids (viral protein corona) which influences infectivity and immune cell activation. We also show that viruses can act as nanosurface catalysts for the aggregation of amyloid peptides such as amyloid beta which is involved in Alzheimer's disease. Our results highlight the important role of viral extracellular interactions in viral pathogenicity and demonstrate a novel link between viral and protein aggregation diseases.

Introduction

The term "protein corona" refers to the layer of proteins that adhere to the surfaces of nanostructures when they encounter biofluids. Nanoparticles adsorb biomolecules in complex biological fluids due to the high free energy of their nanosurfaces (1). The importance of the corona layer stems from the fact that it constitutes the actual surface of interaction with biological membranes or "what the cell sees" in the in-vivo context (2). Tens to hundreds of proteins have been found to form the rich and unique biological identity of different nanoparticles in different microenvironments depending on their size, chemistry and surface modification (reviewed in (3–5)). These factors were found to be critical determinants of the biodistribution and pharmacodynamics of nanoparticles (6). On the other hand, the ability of the surfaces of nanoparticles to partially denature certain corona proteins exposing "cryptic epitopes" highlights the role of the protein corona in the toxicology of nanoparticles (7). This process is particularly important in the context of nanoparticle interaction with amyloidogenic peptides such as amyloid beta (Aβ), α-synuclein and islet amyloid poly peptide (IAPP), which are involved in human diseases such as Alzheimer's disease, Parkinson's disease and diabetes mellitus type 2 disease, respectively. Nanoparticles have been shown to catalyze amyloid formation via binding of amyloidogenic peptides in their corona, thereby increasing local peptide concentration and inducing conformational changes that facilitate β-sheet stacking and fiber formation (8, 9). This surface-assisted nucleation has been demonstrated with several nanoparticles with different amyloidogenic peptides including β2-microglobulin, IAPP, Aβ42 and α-synuclein (8–10). Similarly, this catalytic process was shown to be dependent on particle size, curvature and surface chemistry (9, 10).

Here, we studied viruses in terms of their biophysical equivalence to synthetic nanoparticles in extracellular environments. As nanosized obligate intracellular pathogens, viruses lack replicative capacity outside the cell, and are thus expected to interact with host factors in the microenvironment in ways that are similar to synthetic nanoparticles. In the current work we used the well-established techniques of nanotechnology to study the nanosurface protein interactions of infectious viruses. We investigated the protein corona of respiratory syncytial virus (RSV) in different biofluids and its influence on viral infectivity and immune cell activation. Additionally, we studied the interaction of both RSV and HSV-1 with amyloidogenic peptides.

RSV is an enveloped orthopneumovirus with a diameter between 100 to 300 nm and a single stranded negative-sense RNA genome with 10 genes encoding 11 proteins (11, 12). It is a leading cause of acute lower respiratory tract infections in young children worldwide causing up to an annual estimate of 34 million acute infections in the lower respiratory tract (13). By the first year of life, nearly 70% of children get infected with RSV at least once; and this percentage rises up to 90% by the second year of age causing up to 196,000 yearly fatalities (14). Reinfection with RSV occurs throughout life usually with mild symptoms of uncomplicated upper respiratory tract infection (15). However, reinfection in the elderly and immunocompromised individuals can lead to severe disease. While natural infection leads to the production of neutralizing antibodies, the ability of these antibodies to protect from subsequent RSV infections appear to be incomplete (16, 17). Neither a vaccine nor an antiviral therapy is yet available except for passive immunization using anti-RSV monoclonal antibody, palivizumab, which reduces RSV-associated hospitalization by 55% in infants at high risk (18, 19). Early vaccine trials using formalin-inactivated RSV led to enhanced disease with up to 80% of vaccinees being hospitalized and two dying

(15, 17). This led to the hypothesis that the host immune responses play an important role in RSV disease pathophysiology.

HSV-1 is an example of another virus with very high prevalence, infecting nearly 70% of the human population (20). Unlike RSV, it is a double-stranded DNA virus consisting of an icosahedral nucleocapsid surrounded by tegument and envelope with virion size ranging from 155 to 240 nm (21). HSV-1 is a neurotropic virus that infects peripheral sensory neurons and establishes latency (22). Latent HSV-1 gets occasionally reactivated causing peripheral pathology and under certain circumstances it can migrate into the central nervous system causing herpes simplex encephalitis; the most common cause of sporadic fatal viral encephalitis (22, 23). In the context of the current work we focus on the presumptive role of HSV-1 in the pathology of Alzheimer's disease (AD) (24). A number of risk factors have been associated with AD including the E4 allele of the apolipoprotein E (APOE), diabetes, vascular pathology, neuroinflammation and infections (25). Among the infections that have been implicated in AD, several recent studies have supported the theory of a major role of HSV-1 in AD (24). HSV-1 DNA has been found to be specifically localized in AD amyloid plaques. In AD brains, 80% of the amyloid plaques contained HSV-1 DNA, while only 24% of the viral DNA was associated with plaques in normal aged brains (26). Additionally, the presence of anti-HSV IgM antibodies which indicate HSV reactivation is correlated with a high risk of AD (27). Moreover, HSV-1 infection has been shown to promote neurotoxic Aβ accumulation in human neural cells and to the formation of Aβ deposits in the brains of infected mice (28). Despite these correlations, to our knowledge, no evidence has been found supporting a direct role of HSV-1 in the process of amyloid aggregation.

In the present study, we demonstrated that upon encountering different biofluids, RSV accumulated an extensive and distinct protein corona that was biofluid-dependent. RSV infectivity and capacity to activate moDCs was significantly affected by the different coronas. Moreover, upon interaction with an amyloidogenic peptide derived from IAPP, RSV accelerated the process of amyloid aggregation via surface-assisted nucleation. This amyloid catalysis was also demostrated for HSV-1 and $A\beta_{42}$ peptide. Our data highlight the importance of viral protein corona interactions for viral pathogenesis and the direct mechanistic overlap between viral and amyloid pathologies.

Results

RSV accumulates distinctive protein coronas in different biological fluids

Based on the extensive literature describing the significant role of corona factors in synthetic nanoparticle functionality, we used the established techniques to answer questions relevant to RSV pathogenicity (29). Using proteomics, the RSV protein corona profile in human plasma (HP), human bronchoalveolar lavage fluid (BAL), rhesus macaque monkey plasma (MP), and fetal bovine serum (FBS) was assessed. These biofluids represent different microenvironments encountered by the virus in terms of tissue tropism (HP vs. BAL), zoonosis (MP) and culturing conditions (FBS). Viral stocks were produced in serum-free conditions to prevent initial contamination with FBS proteins. Serum-free produced virions were incubated with 10% v/v solutions of FBS, HP, MP and BAL in serum-free medium with 10 mM sodium citrate to prevent clotting in the plasma samples. After incubation for 1 h at 37 ˚C, the virions were reharvested by centrifugation and washed twice before performing proteomic analysis. Controls included uninfected cell medium representing the background cellular

secretome and synthetic nanoparticles of a size comparable to RSV (200 nm) with positively-charged amine groups or negatively-charged carboxylate groups on their surface. Analysis of proteomics data by principle component analysis (PCA) showed that viral samples were well separated from the control samples with tight replicate groupings (Fig. 1A). The analysis also revealed an extensive and unique protein corona signature for viral samples in each biological fluid. While the serum-free viral particles contain some host factors that are incorporated during virus replication and budding from the cells, RSV accumulated a different set of host factors which were dependent on the biofluid (Fig. 1B). Proteomics data were visualized by heat map and hierarchical clustering which separated groups depending on the pre-coating biofluid, suggesting that the proteomic identity of viral particles depended on the microenvironment (Fig. 1C). As such, a characteristic protein fingerprint was associated with each biological fluid. The viral corona factors present in each biofluid are listed in Supp. Table 1. Additionally, transmission-electron microscopy (TEM) was used in order to visualize the viral corona layer. A fuzzy layer of factors is seen interacting with the viral surface during cell membrane encounter in HP and FBS conditions, which was absent in serum free conditions (Fig. 1D and Supp. Fig. 1).

Protein corona influences viral infectivity and monocyte derived dendritic cells (moDC) activation

To investigate if differential corona composition affects viral infectivity serum-free produced virions were pre-incubated with different biofluids before infection of HEp-2cells. The RSV virions produced in serum-free medium were incubated with biofluids at a protein concentration of 0.3 mg/ml (equivalent to 5% v/v) for 1 h at 37 ˚C then diluted 10 times in serum-free medium before adding to the cells at final MOI of 1. Corona pre-coating had a significant effect on viral infectivity as demonstrated by the differential frequency of eGFP expressing cells quantified by flow cytometry (Fig. 2A and 2B). HP corona pre-coating significantly reduced infectivity compared to serum-free conditions, while FBS and MP led to 5-6 fold enhancement in infectivity. BAL corona also enhanced infectivity, but to a lower extent as compared to MP and FBS. Moreover, fluorescence microscopy revealed syncytia formation of cells infected with BAL, MP and FBS coronas (Figure 2 and Supp. Fig. 2).

Furthermore, we investigated the effect of different coronas on the activation of human monocyte-derived dendritic cells (moDCs) by quantifying the expression of the maturation marker CD86. Differentiated moDCs were infected by serum-free produced virions with different corona pre-coatings for 4h in serum-free conditions. The cells were then washed and incubated in full medium for 72h prior to flow cytometry analysis. Only the BAL pre-coated virions were able to induce moDC activation and increase CD86 expression to levels similar to the TLR3 ligand polyI:C (Fig. 2D). BAL only and RSV only did not activate the cells. Additionally, BAL pre-coating enhanced RSV infectivity in moDCs as demonstrated by enhanced eGFP expression (Fig. 2E). In separate experiments, moDCs were incubated with corona pre-coated RSV in serum-free conditions for 48h. Similarly, only BAL pre-coated virions were able to increase CD86 expression despite the higher baseline expression due to prolonged exposure to serum-free conditions (Supp. Fig. 3A). Additionally, moDC activation was dependent on the BAL concentration at fixed viral MOI (Supp. Fig. 3B). Altogether, this shows that preincubation of serum-free produced virions in different biofluids to allow a corona formation greatly affects infectivity and the ability to induce moDC activation.

Differential RSV corona composition

As a virus that infects nearly 100% of the human population, it is expected that anti-RSV antibodies would be present in biofluids of human origin. Indeed, both HP and BAL contained high levels of anti-RSV IgG antibodies as demonstrated by ELISA analysis (Supp. Fig. 4). The set of factors that were only present in the HP corona and not in the other conditions comprised several antibodies and complement factors including: Ig gamma-1 chain C region, Ig kappa chain C region, Ig gamma-3 chain C region, complement C1q subcomponent subunit C, C4b-binding protein alpha chain, properdin, Ig alpha-1 chain C region, Ig lambda chain V-IV, Ig kappa chain V-III region SIE, complement C1q subcomponent subunit B, protein IGHV3OR16-9, complement component C8 alpha chain, and complement factor H-related protein 5. Moreover, gene list enrichment analysis of HP corona revealed an enrichment of immunological gene ontology (GO) terms such as complement activation and humoral immune response (Fig. 3). The HP corona proteomic profile was consistent with the observed inhibition of infectivity (neutralization), which demonstrates that our corona characterization methodology is representative of the actual layer of host factors that surrounds the viral particle. Moreover, in HP-containing medium the RSV was surrounded by a denser corona layer compared to the FBS conditions lacking the anti-RSV antibodies (Figure 1D and Supp. Fig. 4). Factors from the FBS seemed to bind more loosely compared to HP conditions; however they can still contribute to viral-cell interactions as demonstrated in Figure 2C. While the affinity of such interaction is expected to be lower than that of a specific antibody, it still had a significant effect on viral infectivity as shown in figure 2A and B.

Notably, despite having comparably high levels of virus-specific IgG antibodies, BAL imparted opposite effects on infectivity compared to HP, which we speculate is related to different viral corona composition. On the proteomics level, GO analysis revealed that the viral BAL corona comprised a different set of factors that are less enriched in immunological components and more enriched in factors related to adhesion, anchoring, protein targeting to membrane, interspecies interaction, mutualism through parasitism, protein complex binding, and macromolecular complex binding (Fig. 3). Some unique factors that are only present in the BAL corona include: pulmonary surfactant-associated protein A2 and B, nucleolin, neuroplastin, cadherin-13, tetraspanin, galectin-3-binding protein, isoform 3 of integrin alpha-V, junction plakoglobin, alpha-2-HS-glycoprotein (Fetuin), HLA class I histocompatibility antigen, HLA class I histocompatibility antigen cw-7 alpha chain, hsc70-interacting protein, histone H3, amino acid transporter, protein S100-A10, isoform gamma of poliovirus receptor, isoform 7 of coxsackievirus and adenovirus receptor, isoform 2 of major prion protein, lupus la protein, and isoform 2 of zinc finger CCCH-type antiviral protein 1 (highlighted in Fig. 3 and complete list in Supp. Table 2). On the other hand, both FBS and MP enhanced viral infectivity several folds over serum-free conditions in HEp-2 cells. GO analysis revealed that they are also enriched in terms such as anchoring, adhesion, receptor binding, protein complex binding, unfolded protein binding, interspecies interaction, viral process, and mutualism through parasitism (Supp. Fig. 5). Examples of proteins unique to FBS include: C4b-binding protein alpha-like, beta-2-glycoprotein 1 (apolipoprotein H), hepatitis A virus cellular receptor 1, hsp90 co-chaperone Cdc37, apolipoprotein A-II, coagulation factor V, glia-derived nexin, cytoskeleton-associated protein 4, complement C4 and isoform 2 of fermitin family homolog 2. In MP, the unique factors include: tetraspanin, fibrinogen alpha chain, integrin beta, C-X-C motif chemokine, tubulin beta chain, MHC class I protein, MHC class I antigen, fibronectin isoform 4 preproprotein, fermitin family homolog 3 short form, serum-spreading factor (vitronectin),

vinculin isoform VCL, clusterin, apolipoprotein A-I, coagulation factor XIII A, platelet endothelial cell adhesion molecule, CD59 glycoprotein preproprotein, transferrin, zyxin, heat shock protein beta-1, endothelial cell-selective adhesion molecule, isoform 2 of bone marrow stromal antigen 2, and amyloid beta A4 protein. Full lists of unique factors for all biofluids are found in Supp. Table 2.

RSV catalyzes amyloid aggregation

Since nanoparticles are known to bind amyloidogenic peptides in their coronas leading to induction of amyloid aggregation, we next investigated whether viruses are also capable of binding amyloidogenic peptides and affect their aggregation kinetics. We thus investigated the interaction of RSV with a model amyloidogenic peptide (NNFGAIL) derived from the IAPP. We traced the ability of RSV to accelerate amyloid kinetics using the well-established thioflavin T (ThT) based methodology. The ThT dye changes its fluorescence emission spectrum upon binding to amyloid fibrils, and plotting relative changes in the fluorescence intensity against time illustrates the kinetics of the amyloid formation process (30). Using the ThT assay, we found that the presence of RSV particles significantly accelerated amyloid formation of NNFGAIL compared to uninfected cell media (Fig. 4A). Extensive fiber networks are observed with TEM within 100 min. of incubation with RSV with virions located at the tip of some of these fibers (Fig. 4B). This demonstrates that RSV can act as catalytic nanosurface for amyloid catalysis. It also serves as a proof-of-concept for the ability of viruses to bind peptides in their corona and to induce partial misfolding to the bound factors. On the other hand, RSV failed to catalyze the amyloid aggregation of GNNQQNY peptide, which is derived from yeast prion protein. This, in turn, shows that such interactions are not universal to all amyloidogenic peptides but rather selective depending on the virus/peptide pair.

HSV-1 accelerates the kinetics of $A\beta_{42}$ amyloid formation

The finding that viral nanosurfaces can serve as catalysts for amyloid formation warranted further investigation in clinically relevant systems. To this end, we chose HSV-1 and $A\beta_{42}$ peptide, whose aggregation is a major hallmark of AD. Recently, there has been an increasing body of reports suggestive of a correlation between HSV-1 infection and AD, reviewed in (24); however, evidence of a direct role of HSV-1 in the process of amyloid nucleation and subsequent fibril growth is currently lacking.

We found that HSV-1 significantly accelerated amyloid formation of $A\beta_{42}$ compared to uninfected cell medium (Fig. 5A). Amyloid fiber formation started within minutes in the presence of viral particles, while it took more than 5 h of lag time for the process to start in the controls (Fig. 5A). Nucleation catalysis took place only in the virus-containing medium despite the presence of other particulate species in the controls such as lipoprotein particles and extracellular vesicles. Additionally, we found that the catalytic effect is dependent on viral concentration showing that the presence of a sufficient amount of viral particles is critical for the catalytic process (Fig. 5B). Importantly, while the virus imparts its catalytic activity at about $2x10^7$ PFU/ml, amine-modified nanoparticles of comparable size start demonstrating activity at a concentration of $1x10^{10}$ particles/ml (Fig. 5C). This shows that viral particles have a greater ability to mediate the catalytic nucleation at several orders of magnitude lower concentration compared to synthetic nanoparticles. Additionally, the propensity of HSV-1 mediated amyloid catalysis is higher for the more amyloidogenic $A\beta_{42}$ peptide compared to the shorter, less amyloidogenic $A\beta_{40}$ peptide (Fig. 5D).

Amyloid induction was further confirmed by TEM demonstrating fibril formation within 100 mins. of incubation with viral particles (Fig. 5E-J). Amyloid protofilaments and fibrils at different stages of elongation can be seen interacting with the viral surface. Fig. 5E and F show multiple fibrillary structures emerging from one viral particle. An aggregated species is located at the connection between the viral surface and the fibrils, as shown in Fig. 5F and G. This suggests that a nucleation mechanism takes place on the surface, thereby sparking fibril elongation. Viral particles also interact with fibrillar structures that are part from an extensive network of fibers as shown in Fig. 5H and 5I. Interestingly, Fig. 5J demonstrates a ladder-pattern of fibrils, which might implicate a propagative catalytic mechanism where a single virion starts several amyloidogenic reactions in tandem. Nanoparticles are also shown to produce amyloid fibrils of similar morphology to those produced by HSV-1 (Supp. Fig. 6).

Discussion

Viruses rely on the host cellular machinery for replication, production of viral proteins and viral assembly. However, outside cells, viruses cannot replicate; and hence, very similar to nanoparticles except for their bioorganic nature. Based on this biophysical equivalence, viruses are expected to accumulate a rich and selective protein corona layer in extracellular environments similar to nanoparticles. Examples of particular host factors that bind to viral surfaces have previously been described. For example, lipoproteins such as apolipoprotein E (APO E) were shown to be essential for hepatitis C virus (HCV) infection (31). Furthermore, coagulation factors such as factor X were shown to directly bind adenovirus leading to liver tropism (32, 33). Other soluble components such as Gas6 were shown to contribute to the infectivity of lentiviral vectors even when pseudotyped with multiple types of envelope proteins (34). Additionally, soluble heparin sulfonated proteoglycans (HSPGs) were shown to enhance the infectivity of human papillomavirus (HPV) (35). Interestingly, amyloids derived from prostatic acidic phosphatase (PAP) in semen were shown to enhance HIV-1 infectivity by several orders of magnitude (36). These studies demonstrate the significant role of host proteins that adhere to viral surfaces; however, to our knowledge, there is no work that has comprehensively studied and characterized the entire corona of a virus in different biofluids.

In this work, we used proteomics to study protein corona enrichment on the surface of RSV in different biofluids. We investigated the RSV protein corona in biofluids that are relevant to viral tropism, zoonosis and culturing conditions. As RSV is a virus tropic to the respiratory tract, we compared the viral corona in human BAL versus HP from young healthy volunteers. We also investigated the RSV corona in plasma from rhesus macaque monkeys which are used as models for RSV study and vaccine development (37). RSV was initially discovered in monkeys and the risk of transmission between humans and monkeys is documented in captive non-human primates (38, 39). Additionally, we studied the corona in FBS which is the most commonly used cell growth supplement for viral production and *in-vitro* studies.

Using mass spectrometry-based proteomics we found that RSV accumulated different protein coronas depending on the biofluid. PCA showed that different RSV groups were separable from one another and from control nanoparticles of similar size (Fig. 1). While the corona layer of nanoparticles is dependent on the size, surface chemistry and charge, for viruses it is a more composite function of glycoproteins and lipids, in addition to

surface curvature and charge. Being also subject to optimization through selection pressure, we speculate that the viral protein corona would be more specific than that of nanoparticles.

The protein corona layer was visualized using TEM which revealed a fuzzy layer surrounding the viral surface involved in cellular interactions (Fig. 1D). Functionally, the coronas from the different biofluids enhanced infectivity except for the HP corona. In accordance with the biological activity, proteomic analysis of the HP corona showed that it is enriched in antibodies and complement factors and TEM demonstrated a denser, more compact corona layer (Fig. 1D & Fig. 3). An added advantage of the corona fingerprinting technique is that it allows for an unbiased and comprehensive characterization of the components of the protein complex involved in RSV neutralization, something that can reveal additional functionally important factors. The BAL corona on the other hand enhanced viral infectivity in both HEp-2 cells and moDCs despite having equally high anti-RSV IgG antibody titers as compared to HP. The BAL corona profile was different including proteins that are related to membrane localization, interspecies interaction and adhesion (Fig. 3). This suggests that, despite high antibody titers, the neutralization complex might not be forming as efficiently in BAL as compared to HP, which might explain the ability of RSV to cause pulmonary reinfection even in individuals with high IgG titers (16). Additionally, BAL preincubation was the only condition that induced moDC activation (Fig. 2 and Supp. Fig. 3) demonstrating a role of corona factors in virus-induced immune activation that may contribute to disease pathophysiology. The list of proteins that are uniquely detected in the BAL corona included pulmonary surfactants which have been shown to enhance RSV infectivity (40), nucleolin which has been shown to be important for RSV cell entry (41), adhesion molecules (such as tetraspanin, neuroplastin, integrin and cadherin), immune modulators (such as HLA class I histocompatibility antigen), and zinc finger CCCH-type antiviral protein 1. Taken together, this shows that extracellular RSV can interact with microenvironmental factors forming a “viral corona”. As the corona layer is a rich and complex layer, the final biological effect is expected to be dependent on a multitude of corona factors rather than a single protein. Moreover, it is not the combination of the proteins in the biofluids per se that affect the outcome but rather the protein layer building up around the virus, as shown by the lack of moDC activation by BAL fluid alone (Fig. 2).

Other fluids investigated in our study included FBS and MP and they both enhanced the infectivity of RSV. GO analysis suggests a role of these factors in interspecies interaction, mutualism, viral process, protein complex binding, unfolded protein binding anchoring and adhesion. Factors in FBS that can be contributing to these effects include C4b-binding protein alpha-like which is a complement inhibitor, lipoproteins such as apolipoprotein H and apolipoprotein A-II, isoform 2 of fermitin family homolog 2 which binds to membranes enriched in phosphoinositides and enhances integrin-mediated adhesion (42), hepatitis A virus cellular receptor 1, and coagulation factor V as some members of the coagulation cascade were reported to enhance viral infectivity (43). In the MP corona, lipoproteins such as apolipoprotein A-I and clusterin (apolipoprotein J) are found. Recently, apolipoprotein J was shown to be enriched in the corona of polyethylene glycol modified nanoparticles and to functionally reduce uptake into macrophages (44). Additionally, several adhesion proteins are found in the MP corona including: fibronectin isoform 4 preproprotein, platelet endothelial cell adhesion molecule, endothelial cell-selective adhesion molecule, fermitin family homolog 3 short form, vinculin isoform VCL, and zyxin. The MP corona also includes receptor ligands such as: transferrin and C-X-C motif chemokine, complement regulators such as: vitronectin and CD59 glycoprotein preproprotein together with coagulation

factor XIII A and tetherin (isoform 2 of Bone marrow stromal antigen 2) which possesses antiviral properties based on its ability to tether viruses to the cell membrane preventing their release (45). Taken together, this illustrates that the observed functional effects of the viral protein corona is most likely mediated by a combination of factors that are enriched on the viral surface and not by a single factor. Since many viruses bind to several receptors and co-receptors, such interactions might be taking place in a multivalent manner (46).

Notably, our results on FBS and MP show that viral pre-coating with a protein corona via simple exposure to low concentrations of biofluids from different species can have a dramatic impact on infectivity. It highlights that viral protein corona has to be taken into consideration in relation to zoonotic studies and development of animal models, as well as viral culturing for research or vaccine purposes. Rhesus macaques have been used as models for RSV, and transmission from humans to captive primates has been reported, sometimes leading even to death (39, 47). The species-specific corona signature may contribute, together with other factors, to differences in virulence and disease severity across species. Moreover, corona factors can contribute to viral tolerance in animal reservoirs such as monkeys, bats and birds. Additionally, mutations that lead to enrichment of a different corona in a particular host may lead to zoonotic crossing of species barriers. Extracellular host factors are the site of viral first encounter, and positive selection can act in the direction of optimized corona enrichment if it enhances viral replicative fitness. This is particularly important to understand in the context of emerging viral infections. On the other hand, a large proportion of emerging viruses do not propagate well in cell culture (48). These unculturable viruses are very challenging in terms of study or vaccine/antiviral development. Utilizing corona factors from reservoir hosts or changing the source of biofluid, as shown here, may have a positive impact on growing viruses in cell culture for vaccine and research purposes.

Moreover, to investigate whether viral nanosurface interactions with host factors involves surface-assisted nucleation, we incubated RSV with a model amyloidogenic peptide derived from IAPP; NNFGAIL. We found that RSV accelerated the kinetics of amyloid aggregation, demonstrating that a viral particle, similar to a synthetic nanoparticle, is capable of amyloid catalysis via surface-assisted nucleation. Interestingly, amyloidogenic peptides can also be found in the RSV corona profile in BAL (isoform 2 of major prion protein) and in MP (amyloid beta A4 protein). This shows that viral interaction with amyloidogenic peptides is feasible in complex biological fluids.

In order to investigate if this catalytic mechanism extends to other virus/amyloid pairs of more clinical relevance, we tested if HSV-1 could accelerate the amyloid kinetics of $A\beta_{42}$ which is implicated in AD. Several recent studies have suggested HSV-1 involvement in AD (24). Similarly, we found that HSV-1 dramatically accelerates the kinetics of amyloid aggregation of $A\beta_{42}$ but not $A\beta_{40}$, better than nanoparticles and in a threshold-dependent manner (Fig. 5). Additionally, TEM demonstrated a clear interaction between amyloid fibrils at different stages of maturation and the viral surface via some aggregate intermediate, which we speculate represent the surface-assisted nucleation process. Moreover, ladder-patterns of short fibers were observed, which might indicate that the virus can catalyze several reactions by carrying the amyloid nucleus on its surface.

Taken together, our data on RSV and HSV-1 presented here demonstrate that viruses can physically act as nanosurfaces that catalyze amyloid nucleation leading to accelerated fibril formation. This provides a direct mechanistic link between viral and amyloid pathologies and shows that the two modes of pathogenesis can

closely overlap. Our data suggests that viruses can contribute to both the initiation and propagation of amyloid pathologies. The ability of viruses to replicate and become released in large quantities can lead to amyloid precipitation due to the sudden availability of vast nanosurfaces in a particular infected microenvironment. Additionally, due to the documented stability of such surface interactions, viruses might be able to carry amyloidogenic nuclei (seeds) on their surfaces leading to propagation within a host and between different hosts across the viral infective cycle. Further understanding of these interactions can provide new insights into the pathogenic formation of amyloid aggregates in AD and other protein aggregation diseases and open up new avenues for drug development. Moreover, the implication that viruses are capable of inducing conformational changes in bound host factors leading to exposure of cryptic epitopes may prove important for better understanding the correlation between viruses and autoimmune diseases.

To conclude, the current work is based on the biophysical equivalence between viruses and synthetic nanoparticles in extracellular environments. We demonstrated that nanotechnological concepts such as the protein corona and surface-assisted nucleation can be extended to infectious viruses leading to novel insights on viral-host interactions. We showed that viral protein corona accumulation and amyloid catalysis are two aspects of the same phenomenon, namely viral nanosurface interaction with extracellular host proteins (Fig. 6). This can lead to the modulation of how viruses interact with cells and/or the induction of conformational changes in bound proteins that leads to accelerated amyloid aggregation. These results highlight the critical role of viral extracellular interactions in viral infectivity and in relation to extracellular protein pathology.

References

1. Monopoli MP, Aberg C, Salvati A, Dawson K a (2012) Biomolecular coronas provide the biological identity of nanosized materials. *Nat Nanotechnol* 7(12):779–86.

2. Walczyk D, Bombelli FB, Monopoli MP, Lynch I, Dawson KA (2010) What the cell “sees” in bionanoscience. *J Am Chem Soc* 132(16):5761–5768.

3. Lee B (2017) Protein corona : a new approach for nanomedicine design. 3137–3151.

4. Neagu M, et al. (2016) Protein bio-corona: critical issue in immune nanotoxicology. *Arch Toxicol*:1–18.

5. Ke PC, Lin S, Parak WJ, Davis TP, Caruso F (2017) A Decade of the Protein Corona. *ACS Nano* (Figure 1):acsnano.7b08008.

6. Caracciolo G, Farokhzad OC, Mahmoudi M (2016) Biological Identity of Nanoparticles In Vivo : Clinical Implications of the Protein Corona. *Trends Biotechnol* xx:1–8.

7. Lynch I, Dawson KA, Linse S (2006) Detecting Cryptic Epitopes Created by Nanoparticles. *Sci STKE* 2006(327):pe14-.

8. Gladytz A, Abel B, Risselada HJ (2016) Gold-Induced Fibril Growth: The Mechanism of Surface-Facilitated Amyloid Aggregation. *Angew Chemie Int Ed*:1–6.

9. Terakawa MS, Yagi H, Adachi M, Lee YH, Goto Y (2015) Small liposomes accelerate the fibrillation of

amyloid beta (1- 40). *J Biol Chem* 290(2):815–826.

10. Mahmoudi M, Kalhor HR, Laurent S, Lynch I (2013) Protein fibrillation and nanoparticle interactions: opportunities and challenges. *Nanoscale* 5(7):2570–88.

11. Bächi T, Howe C (1973) Morphogenesis and ultrastructure of respiratory syncytial virus. *J Virol* 12(5):1173–80.

12. Radhakrishnan A, et al. (2010) Protein analysis of purified respiratory syncytial virus particles reveals an important role for heat shock protein 90 in virus particle assembly. *Mol Cell Proteomics* 9(9):1829–1848.

13. Nair H, et al. (2010) Global burden of acute lower respiratory infections due to respiratory syncytial virus in young children: a systematic review and meta-analysis. *Lancet* 375(9725):1545–1555.

14. McDermott DS, Weiss KA, Knudson CJ, Varga SM (2011) Central role of dendritic cells in shaping the adaptive immune response during respiratory syncytial virus infection. *Futur Virol* 6(8):963–973.

15. Collins PL, Graham BS (2008) MINIREVIEW Viral and Host Factors in Human Respiratory Syncytial. 82(5):2040–2055.

16. Hall CB, Walsh EE, Long CE, Schnabel KC (1991) Immunity to and frequency of reinfection with respiratory syncytial virus. *J Infect Dis* 163(4):693–698.

17. Graham BS (2011) Biological Challenges and Technological Opportunities for RSV Vaccine Development. *Immunol Rev* 239(1):149–166.

18. Cardenas S, Auais A, Piedimonte G (2005) Palivizumab in the prophylaxis of respiratory syncytial virus infection. *Expert Rev Anti Infect Ther* 3(5):719–26.

19. Kim L, et al. (2017) Identifying gaps in respiratory syncytial virus disease epidemiology in the United States Prior to the introduction of vaccines. *Clin Infect Dis* 65(6):1020–1025.

20. Roizman B (2007) *Human Herpesviruses: Biology, Therapy and Immunoprophylaxis* doi:10.2277/0521827140.

21. Laine RF, et al. (2015) Structural analysis of herpes simplex virus by optical super-resolution imaging. *Nat Commun* 6:5980.

22. Menendez CM, Carr DJJ (2017) Defining nervous system susceptibility during acute and latent herpes simplex virus-1 infection. *J Neuroimmunol* 308:43–49.

23. Zuo X, Tang W, Chen X, Huang W (2017) A review with comments on herpes simplex encephalitis in adults. 24–27.

24. Piacentini R, et al. (2014) HSV-1 and Alzheimer's disease: More than a hypothesis. *Front Pharmacol* 5 MAY(May):1–9.

25. Santos CY, et al. (2017) Pathophysiologic relationship between Alzheimer's disease, cerebrovascular disease, and cardiovascular risk: A review and synthesis. *Alzheimer's Dement Diagnosis, Assess Dis Monit* 7:69–87.

26. Wozniak MA, Itzhaki RF (2010) Herpes simplex virus type 1 DNA is located within Alzheimer's disease amyloid plaques. *J Pathol* 220(September):114–125.

27. Lövheim H, Gilthorpe J, Adolfsson R, Nilsson L-G, Elgh F (2014) Reactivated herpes simplex infection increases the risk of Alzheimer's disease. *Alzheimers Dement* 11:1–7.

28. Wozniak MA, Itzhaki RF, Shipley SJ, Dobson CB (2007) Herpes simplex virus infection causes cellular beta amyloid accumulation and secretase upregulation. *Neurosci Lett* 429(2–3):95–100.

29. Tenzer S, et al. (2013) Rapid formation of plasma protein corona critically affects nanoparticle pathophysiology. *Nat Nanotechnol* 8(10):772–81.

30. Arosio P, Knowles TPJ, Linse S (2015) On the lag phase in amyloid fibril formation. *Phys Chem Chem Phys* 17(12):7606–7618.

31. Chang K-S, Jiang J, Cai Z, Luo G (2007) Human apolipoprotein e is required for infectivity and production of hepatitis C virus in cell culture. *J Virol* 81(24):13783–13793.

32. Waddington SN, et al. (2008) Adenovirus serotype 5 hexon mediates liver gene transfer. *Cell* 132(3):397–409.

33. Doronin K, et al. (2012) Coagulation factor X activates innate immunity to human species C adenovirus. *Science* 338(6108):795–8.

34. Morizono K, et al. (2011) The soluble serum protein Gas6 bridges virion envelope phosphatidylserine to the TAM receptor tyrosine kinase Axl to mediate viral entry. *Cell Host Microbe* 9(4):286–98.

35. Surviladze Z, Dziduszko A, Ozbun MA (2012) Essential roles for soluble virion-associated heparan sulfonated proteoglycans and growth factors in human papillomavirus infections. *PLoS Pathog* 8(2). doi:10.1371/journal.ppat.1002519.

36. Münch J, et al. (2007) Semen-Derived Amyloid Fibrils Drastically Enhance HIV Infection. *Cell* 131(6):1059–1071.

37. Taylor G (2017) Animal models of respiratory syncytial virus infection. *Vaccine* 35(3):469–480.

38. BLOUNT RE, MORRIS JA, SAVAGE RE (1956) Recovery of cytopathogenic agent from chimpanzees with coryza. *Proc Soc Exp Biol Med* 92(3):544–549.

39. Szentiks CA, Ko S, Silinski S, Speck S, Leendertz FH (2009) Lethal pneumonia in a captive juvenile chimpanzee (Pan troglodytes) due to human-transmitted human respiratory syncytial virus (HRSV) and infection with Streptococcus pneumoniae. 38:236–240.

40. Hickling TP, et al. (2000) Lung surfactant protein A provides a route of entry for respiratory syncytial virus into host cells. *Viral Immunol* 13(1):125–135.

41. Tayyari F, et al. (2011) Identification of nucleolin as a cellular receptor for human respiratory syncytial virus. *Nat Med* 17(9):1132–1135.

42. Qu H, et al. (2011) Kindlin-2 regulates podocyte adhesion and fibronectin matrix deposition through interactions with phosphoinositides and integrins. *J Cell Sci* 124(6):879–891.

43. Pryzdial ELG, Sutherland MR, Ruf W (2014) The Procoagulant Envelope Virus Surface: Contribution to Enhanced Infection. *Thromb Res* 133:S15–S17.

44. Schöttler S, et al. (2016) Protein adsorption is required for stealth effect of poly(ethylene glycol)- and poly(phosphoester)-coated nanocarriers. *Nat Nanotechnol* (February):1–6.

45. Kuhl BD, Cheng V, Wainberg MA, Liang C (2011) Tetherin and its viral antagonists. *J Neuroimmune Pharmacol* 6(2):188–201.

46. Wickham TJ, Granados RR, Wood H a, Hammer D a, Shuler ML (1990) General analysis of receptor-mediated viral attachment to cell surfaces. *Biophys J* 58(6):1501–1516.

47. McArthur-Vaughan K, Gershwin LJ (2002) A rhesus monkey model of respiratory syncytial virus infection. *J Med Primatol* 31(2):61–73.

48. Pyrc K, et al. (2010) Culturing the unculturable: human coronavirus HKU1 infects, replicates, and produces progeny virions in human ciliated airway epithelial cell cultures. *J Virol* 84(21):11255–11263.

49. Mbiguino a, Menezes J (1991) Purification of human respiratory syncytial virus: superiority of sucrose gradient over percoll, renografin, and metrizamide gradients. *J Virol Methods* 31(2–3):161–70.

Materials and Methods

Viral and cell culture

HEp-2 cells, a human laryngeal carcinoma cell line, were used for RSV viral culture and infectivity experiments. Preparation of RSV A2/eGFP stocks was performed using VP-SFM serum-free, ultra-low protein medium containing no proteins, peptides, or other components of animal or human origin (ThermoFisher, USA). HEp-2 cells were initially seeded in growth medium (DMEM medium with 5% FBS (ThermoFisher, USA), 1% Penicillin/Streptomycin (ThermoFisher, USA) and 0.01M HEPES (SigmaAldrich, Germany) until they reached approximately 70-80% confluency. At the day of infection, the cells were washed twice with warm PBS and the medium was replaced with VP-SFM containing 50 μg/ml gentamycin. Cells were infected at MOI of 4 and incubated for 5-6 days until >90% eGFP expression was visible with fluorescence microscopy. Cells were then scraped, vortexed thoroughly, sonicated for 10 min., vortexed thoroughly one more time and spun at 1000 g for 5 min. The supernatant was transferred to new tubes and used freshly for the proteomics and amyloid interaction

experiments. For long term storage, infectivity and moDC activation experiments the supernatant was adjusted with $MgSO_4$ and HEPES (SigmaAldrich, Germany) solutions to a final concentration of 0.1M $MgSO_4$ and 50 mM HEPES. RSV was then concentrated using a 1.45 M sucrose cushions in the following buffer (1 M MgSO4; 50 mM Hepes, pH 7.5; 150 mM NaC1) according to (49) via centrifugation for 4 h at 7500 g at 4 ˚C. The viral concentrated layer was then harvested from interface between the cushion and the supernatant, aliquoted and immediately frozen at -80 ˚C. Quantifications of viruses were measured using real-time qPCR. Purification of viral RNA was performed using the QIAamp® Viral RNA extraction kit (QIAGEN) and extracted RNA was stored at -80 ˚C. Viral titers were determined using the SuperScript® III Platinum® One-Step Quantitative real-time PCR system (Life Technologies) with the following probe and primers: RSV-A probe CAC CAT CCA ACG GAG CAC AGG AGA T (5'-labeled with 6-FAM and 3' labeled with BHQ1), RSV-A forward primer AGA TCA ACT TCT GTC ATC CAG CAA and RSV-A reverse TTC TGC ACA TCA TAA TTA GGA G. For initial viral quantification purposes, a commercially available RSV-A2 strain was purchased from (Advanced Biotechnologies Inc).

For HSV-1, strain F HSV-1 stocks were prepared by infecting African green monkey kidney (VERO) cells at 80–90% confluency in DMEM (Invitrogen) supplemented with 5% FBS. The virus was harvested 2 d after infection. Cells were subjected to two freeze-thaw cycles and spun at 20,000 g for 10 min to remove cell debris. Clarified supernatant was aliquoted and stored at -80°C until use. Non-infected cell medium was prepared with the same procedure without viral infection. Plaque assay was used to determine viral titers. 10-fold dilutions of virus were added onto VERO cells for 1 h at 37°C, then inoculum was removed, and fresh medium containing 0.5% carboxymethyl cellulose (Sigma Aldrich) was added. Cells were fixed and stained 2d later with a 0.1% crystal violet solution and the number of plaques was counted.

Human BAL samples

The use of human BAL samples for the current study was approved by the Regional Committee for Ethical Review in Stockholm (D. No 2016/1985-32). All donors had given oral and written informed consent to participate in the bronchoscopy study, in line with the Helsinki Declaration. The clinical characteristics of the utilized cohort of healthy volunteers have been described in detail elsewhere (Che KF et al, Am J Resp Crir Care Med 2014). Briefly, healthy subjects of male and female gender were recruited at the Lung Allergy Clinic, Karolinska University Hospital, Solna. These subjects were examined after denying regular tobacco smoking and history of allergy or lung disease during an interview. The final inclusion required that these subjects displayed no signs of pulmonary or disease during clinical examination, spirometry and clinical blood testing including electrolytes, white cell differential counts and C-reactive protein. Bronchoscopy with BAL (5 x 50 ml of sterile and phosphate-buffered saline) was performed according to clinical routine at Karolinska University Hospital, Solna, as previously described (Che KF et al, Am J Resp Crir Care Med 2014). BAL was concentrated using 5 kDa cutoff 4 ml spin concentrator (Agilent Technologies, USA) before infectivity experiments.

Protein corona proteomics

FBS was obtained commercially (ThermoFisher, USA). HP was obtained and pooled from at least 3 different healthy donors. MP was obtained and pooled from at least 3 different Indian rhesus macaques that were RSV

seronegative. Ethical permit Dnr N2 / 15, Institutionen för medicin, Karolinska University Hospital, Solna. For the corona proteomic experiments, freshly-harvested serum-free RSV supernatant (not-sucrose cushion concentrated) containing 6.6 x 10^9 viral genome equivalents was incubated with 10% v/v solutions of different biofluids in VP-SFM medium for 1h at 37 ˚C. Before adding RSV, all the biofluid solutions were adjusted to 10 mM sodium citrate (SigmaAldrich, Germany) to prevent coagulation. As a control, uninfected cell supernatant prepared in a similar way was also incubated with the biofluid solutions. For nanoparticles, 3 x 10^{11} of 200 nm amine- or carboxylate- modified nanoparticles (FluoSpheres™, ThermoFisher USA) were incubated with 10% solutions of biofluids at similar conditions. After incubation, viral/nanoparticle corona complexes were spun at 20,000 g at 4 ˚C, supernatant removed and the pellet resuspended in 1 ml PBS. The pellet was washed twice with PBS using the same centrifugation conditions then boiled at 95 ˚C for 5 min. before measuring the protein content using Micro BCA™ protein assay kit (ThermoFisher, USA). The viral/nanoparticle corona complexes were then resuspended in PBS and adjusted with ammonium bicarbonate to a final concentration of 20 mM. The samples were reduced by addition of 1:20 v/v 100 mM dithiothreitol (DTT) for 45 min. at 56 ˚C, and alkylated with 1:20 v/v 100 mM iodoacetamide (IAA) for 45 min at RT in the dark. Proteins were digested with trypsin (MS gold, Promega) 0,1 µg/µl overnight at 37 °C (trypsin : protein ratio 1:50). The trypsinized proteins were recovered; salts and nonionic detergents were removed using strong cation exchange SCX microcolumns. The microcolumns were initially washed with 100% methanol followed by MilliQ grade water. The samples were adjusted to >0.1% formic acid and then applied to the columns. After washing with 30% methanol and 0.1% formic acid the samples were eluted with 30% methanol and 5% ammonium hydroxide. Samples were dried in a SpeedVac and submitted to mass spectrometry (MS). For MS analysis, samples were dissolved in 10 µL 3% ACN, 0.1% formic acid and analyzed in triplicates. 2 µl were analyzed with a hybrid LTQ-Orbitrap Velos mass spectrometer (ThermoFisher, USA). An Agilent HPLC 1200 system (Agilent) was used to provide the 70 min gradient (unlabeled samples). Data-dependent MS/MS (centroid mode) followed in two stages: first, the top-5 ions from the master scan were selected for collision induced dissociation with detection in the ion trap (ITMS); and then, the same 5 ions underwent higher energy collision dissociation (HCD) with detection in the Orbitrap (FTMS). The data was searched by Sequest under the Proteome Discoverer 1.4.1.1.4 software (ThermoFisher) against the following Uniprot protein sequence databases; bos taurus version 170310, rhesus macaque version 170704, human version 160210 and RSV version 160210 using a 1% peptide false discovery rate cut-off limit. Only proteins present in all three replicates were used in the downstream data analysis.

Data analysis

PCA analysis was performed in R using the prcomp package. Gene list enrichment analysis was performed using ToppFun (Chen J et al.; Nucleic Acids Research 2009). Heatmap visualization and hierarchical clustering was performed using TMeV (Institute for Genomic Research, Rockville, MD, USA). -log10P values are reported (with Bonferroni correction for multiple comparisons).

ELISA

The detection of specific anti-RSV IgG antibodies in biofluids was performed using Human Anti-Respiratory syncytial virus IgG ELISA Kit (ab108765, abcam®, Sweden) according to manufacturer's protocol. All biofluids

(FBS, HP, MP, BAL) were diluted to a protein concentration of 0.3 mg/ml before performing the assay and results were compared to the positive, cutoff, and negative controls provided by the kit manufacturer.

RSV infectivity

HEp-2 cells were seeded in 24-well plates in maintenance medium until they reached 50-60% confluency. On the day of infection, the cells were washed twice with warm PBS and medium was changed to VP-SFM with gentamycin. Before adding to the cells, sucrose cushion-concentrated RSV stocks were preincubated with different biofluids (FBS, HP, MP, BAL) at a final protein concentration of 0.3 mg/ml in VP-SFM with 10 mM sodium citrate for 1 h at 37 ˚C. The corona-precoated viruses were then added to the cells in serum-free conditions (diluted 10x) at a MOI of 1. After 24 h, the medium was changed back to growth medium and cells were visualized with fluorescence microscopy 72 h postinfection. After visualization, the cells were washed and stained with LIVE/DEAD™ Fixable Far Red Dead Cell Stain Kit (ThermoFisher, USA) for 30 min at 4 ˚C in Dulbecco's phosphate-buffered saline (DPBS no calcium, no magnesium, ThermoFisher), then fixed and washed for flow cytometry using Cytofix/Cytoperm™ (BD, USA) according to manufacturer's protocol. Cells were then scraped and resuspended in DPBS, and the data was acquired using MACSQuant® Analyser 10 flowcytometer (Miltenyi Biotec, Sweden). The data was analyzed by FlowJo software (TreeStar) by excluding the dead cells stained with far-red fluorescent dye and subsequent calculation of GFP positive cells within the viable cell population.

MoDC differentiation

Human monocytes were negatively selected from buffy coats using the RosetteSep Monocyte Enrichment Kit (1mL/10mL buffy coat; StemCell Technologies) and differentiated into moDC, using GM-CSF (250ng/mL; PeproTech) and IL-4 (6.5ng/mL; R&D Systems) for 6 days in 37°C, 5% CO_2 at a density of $5x10^5$ cells/mL in RPMI 1640 completed with 10% FCS, 1mM sodium pyruvate, 10mM HEPES, 2mM L-glutamine, and 1% and penicillin/streptomycin (ThermoFisher, USA) as previously described (Sköld et al. Blood, 2012). Immature moDCs were exposed to RSV pre-incubated with different biofluids and then incubated in serum-free conditions as described earlier, and maturation was assessed 48h post treatment using monoclonal antibodies (Abs) to measure expression of the moDC maturation marker CD86 (BD Biosciences). Alternatively, immature moDC were exposed to RSV pre-incubated with different biofluids for 4h, washed and then incubated in full medium for 72 h before analyses of CD86 and RSV-GFP expression. Dead cells were excluded using Live/Dead fixable near-IR dead cell stain kit (ThermoFisher). Flow cytometry sample data were acquired on a Fortessa (BD Biosciences) and the analysis was performed in FlowJo software (TreeStar).

Thioflavin-T Assay

NNFGAIL, GNNQQNY, $A\beta_{42}$, $A\beta_{40}$ were synthesized and purified by Pepscan (The Netherlands) and the final molecular weight was verified by MS. 10 µl of dimethyl sulfoxide (DMSO) (ThermoFisher, USA) were added to 1 mg aliquots of the peptide and running stocks were prepared in MQ water. ThT (Sigma Aldrich) was prepared at 4 mM in MQ water. For the assay, 150 µl/well ThT were added to black clear-bottom 96-well plates (Corning, USA), then 100 µl of freshly-harvested serum-free RSV supernatant (not-sucrose cushion concentrated) , controls, and nanoparticles were added together with 50 µl of the different peptides. ThT fluorescence was

measured at 440 nm excitation and 480 nm emission at 10-15 min. intervals (from bottom with periodic shaking) over 12-24 h on SpectraMax i3 microplate reader (Molecular Devices, USA). Curves were fitted using GraphPad Prism software.

Electron Microscopy

For cell sections with RSV, HEp-2 cells were seeded in 6 cm dishes in maintenance medium until 70-80% confluent, then washed and medium replaced with VP-SFM with gentamycin before infecting with RSV at MOI 100 in serum-free conditions or in 50% FBS or HP. Cells were then fixed with 2.5 % glutaraldehyde in 0.1M phosphate buffer, pH 7.4 at room temperature for 30 min. The cells were scraped of and transferred to an Eppendorf tube and further fixed overnight in the refrigerator. After fixation, cells were rinsed in 0.1M phosphate buffer and centrifuged (100g for 5 min.). The pellets were then fixed with 2% osmium tetroxide (TAAB, Berks, England) in 0.1M phosphate buffer, pH 7.4 at 4 ˚C for 2 h, then dehydrated in ethanol followed by acetone and embedded in LX-112 (Ladd, Burlington, Vermont, USA). Ultrathin sections (approximately 50-60 nm) were cut by a Leica EM UC 6 (Leica, Wien, Austria). Sections were stained with uranyl acetate followed by lead citrate and imaged in a Tecnai 12 Spirit Bio TWIN transmission electron microscope (FEI Company, Eindhoven, The Netherlands) at 100 kV. Digital images were captured by a Veleta camera (Olympus Soft Imaging Solutions, GmbH, Münster, Germany). For cryoimmunoelectron microscopy (iEM), cells were fixed in 3 % paraformaldehyde in 0.1 M phosphate buffer. Samples were then rinsed with 0.1M phosphate buffer and infiltrated in 10% gelatin. Then the specimens were infiltrated into 2.3 M sucrose and frozen in liquid nitrogen. Sectioning was performed at -95˚C and mounted on carbon-reinforced formvar-coated, 50 mesh Nickel grids. Immunolabelling was performed as follows: grids were placed directly on drops of 2% normal goat serum (DAKO, Glostrup, Denmark) in 0.1 M phosphate buffer to block non-specific binding then incubated with the primary antibody (Mouse Anti-RSV fusion protein monoclonal antibody, Millipore, USA) diluted 1:50 in 0.1M of phosphate buffer containing 0.1% normal goat serum overnight in a humidified chamber at room temperature. The sections were washed using the same buffer and bound antibodies were detected using secondary goat-anti-mouse coated with 10 nm gold (BBI solution, Analytic standard, Sweden) at a final dilution of 1:100. Sections were then rinsed in buffer and fixed in 2% glutaraldehyde, stained with 0,05% uranyl acetate, embedded in 1% methylcellulose and then examined in a Tecnai G2 Bio TWIN (FEI company, Eindhoven, The Netherlands) at 100 kV. Digital images were captured by a Veleta camera (Soft Imaging System GmbH, Műnster, Germany). For TEM of viruses with amyloids, 100 µl of RSV (3 x 10^8/ml) or HSV-1 (2 x 10^7/ml) or amine-modified nanoparticles (1 x 10^{10}/ml) were incubated with 50µl 1mM NNFGAIL (for RSV) or 50µM $A\beta_{42}$ (for HSV-1 and nanoparticles) for 100 min. at 37 ˚C. Samples were applied to Formvar/carbon coated 200 mesh nickel grids (Agar Scientific, UK), then negatively stained using an aqueous solution of uranyl acetate (1%) and visualized.

Acknowledgements

We would like to acknowledge the Svenska Sällskapet för Medicinsk Forskning (SSMF) for supporting Kariem Ezzat, Vetenskapsrådet, SSMF, and the Swedish foundation for Strategic Research for supporting Samir EL-Andaloussi, Dr. Michael N. Teng at the University of South Florida for providing the RSV-GFP virus, the service of the Electron Tomography Facility at Karolinska Institutet. Additionally, Anders Lindén obtained project funding from the Swedish Heart-Lung Foundation (No. 20150303), the Swedish Research Council (No.

2016-01653), as well as federal funding from Karolinska Institutet and through the Regional Agreement on Medical Training and Clinical Research (ALF, No. 20140309) between Stockholm County Council and Karolinska Institutet. No funding was obtained from the tobacco industry.

Figure Legends

Figure 1. RSV corona proteomics and electron microscopy. (A) Principal component analysis (PCA) of the corona proteomic profiles of RSV, 200 nm polystyrene nanoparticles amine-modified (NH_2 NPs) or carboxylate-modified (COOH NPs), and uninfected supernatant. Triplicate samples were incubated with 10% solutions of either human plasma (HP), fetal bovine serum (FBS) for 1h at 37 ˚C, then reharvested , washed and finally analyzed by MS (**B**) PCA of the corona proteomic profiles RSV in serum-free conditions (RSV), HP, FBS, MP or BAL triplicate samples prepared and analyzed similarly. (**C**) Heat map representing the viral corona fingerprint of RSV after incubation in different biofluids. Clusters of proteins that are uniquely present to each biofluid pre-coating conditions are marked by the grayscale rectangles on the right according to the following descending order: MP, BAL, FBS, HP. Red and blue indicate higher and lower than mean protein signal respectively. Scale bars represent row Z-scores of $\log_2$ transformed protein signals (**D**) TEM images of HEp-2 cell sections after incubation for 1h with RSV in either serum-free medium (RSV) or medium with 50% HP (RSV+HP) or 50% FBS (RSV+FBS). Compiled images of virions in close proximity to the cell-surface. Black arrows indicate a fuzzy corona layer. Bar = 200 nm.

Figure 2. Different corona pre-coatings affect RSV infectivity and moDC activation. (A) Serum-free produced virions pre-coated with different coronas via pre-incubation with different biofluids at the protein concentration of 0.3 mg/ml for 1h at 37^o C, then added to HEp-2 cells in serum-free medium (diluted 10x) at an MOI of 1. RSV was incubated with the cells for 24h before changing the medium. The frequencies of GFP expressing cells were quantified by flow cytometry 72h post-infection. Representative dot blot graphs are shown. **(B)** Flow cytometry quantification of the GFP positive-cells after RSV pre-coating with different coronas from different biofluids presented as fold-increase over RSV treatment in serum-free conditions. Mean of six replicates. Non-parametric Kruskal-Wallis unpaired test followed by Dunn's post-test or Mann-Whitney test was used to compare the data. P-value: ** $P \leq 0.01$. Statistics were calculated using GraphPad Prism 7 software. (**C**) Representative fluorescence microscopy pictures showing infectivity and syncytia formation in RSV only and RSV+BAL treated HEp-2 cells (**D**) RSV pre-incubated with different biofluids then added to primary moDCs in serum-free conditions at MOI 20 for 4h. Cells were then washed and subsequently cultured in full growth medium for 72h. CD86 expression was quantified by flow cytometry. Representative histograms are shown 1) RSV only 2) polyI:C 3) uninfected control medium 4) FBS only 5) RSV + FBS corona 6) BAL only 7) RSV + BAL corona (**E**) The frequency of RSV-GFP expressing moDC was quantified by flow cytometry 72h post-infection comparing RSV pre-coated with FBS or BAL.

Figure 3. RSV corona proteomic representation. (A) Venn-diagram showing the unique and overlapping protein populations from the RSV corona profiles in different biofluids. The unique factors HP and a selection of unique factors in BAL are shown. (B) Gene list enrichment analysis of the total RSV corona profile in BAL and HP pre-treatment groups. The top five enriched terms are shown in each GO domain.

Figure 4. RSV accelerates the kinetics of amyloid formation. (A) RSV (100 µl of 3 x 10^8 particle/ml stock) incubated with 50 µl of 1mM NNFGAIL peptide and 150 µl of 4 mM ThT solution at 37˚C. (**B**) RSV (100 µl of 3 x 10^8 particle/ml stock) incubated with GNNQQNY peptide. ThT fluorescence was measured at 440 nm excitation and 480 nm emission over 12 h. Controls include uninfected cell supernatant (green), background cell growth medium (blue) and virus only without peptide (grey). Averages and standard deviation of three replicates are shown. (**C-D**) Negatively stained TEM images of RSV incubated with 1 mM NFGAIL for 100 mins. at 37˚C. (**C**) Fibrillar tangles, bar = 5 µM (**D**) RSV virion shown at the base of an amyloid fiber. White arrows indicate viral particle and black arrows indicate fibrillar structures. , bar = 500 nm.

Figure 5. HSV-1 accelerates the kinetics of $A\beta_{42}$ fibrillation and interacts with amyloid fibrils. (A) HSV-1 (100 µl of 2 x 10^7 PFU/ml stock) incubated with 50 µl of 50 µM $A\beta_{42}$ peptide and 150 µl of 4 mM ThT solution at 37 ˚C. ThT fluorescence was measured at 440 nm excitation and 480 nm emission over 24 h. Controls include uninfected cell supernatant (green), background cell growth medium (DMEM + 5% fetal bovine serum – blue) and virus only without $A\beta_{42}$ (grey). (**B**) HSV-1 used at different concentrations. (**C**) HSV-1 (2 x 10^7 PFU/ml stock) and amine-modified polystyrene nanoparticles (dimeter 200 nm, 1 x 10^{10} particles/ml) incubated with $A\beta_{42}$ peptide (**D**) HSV-1 (2 x 10^7 PFU/ml stock) incubated with $A\beta_{42}$ or $A\beta_{40}$ peptides. (**E-J**) Negatively stained TEM images of HSV-1 incubated with 50 µM $A\beta_{42}$ for 100 min. at 37 ˚C. White arrows indicate viral particles and black arrows indicate fibrillar structures. (**E**) Three protofilaments/fibrils stemming from one viral particle, bar = 200 nm. (**F**) Two protofilaments/fibrils stemming from a viral particle interacting with and aggregated structure, bar = 100 nm. (**G**) A viral particle interacting with an aggregate with a long fiber coming out at the interface, bar = 200 nm. (**H**) A viral particle interacting with protofilaments/fibrils which are connected to extensive fibrillar structures, bar =1 µm. (**I**) A rectangular close-up of viral interaction, bar = 500 nm. (**J**) A ladder-pattern of fibrils, bar = 500 nm.

Figure 6. Schematic representation of the different aspects of viral corona interactions. The virus as a nanosurface can interact with the proteins in the extracellular environment enriching particular factors that mediate viral infectivity/signalling via multivalent receptor interaction that involves viral glycoproteins and corona factors. On the other hand, when amyloidogenic peptides bind in the viral corona, viruses are able to catalyze the nucleation process leading to accelerated amyloid kinetics.

Supplementary Figure 1. Immuno-electron microscopy images of RSV in the vicinity of cell surface labelled with anti-F protein antibody, bar = 200 nm.

Supplementary Figure 2. Representative fluorescence microscopy pictures showing infectivity and syncytia formation in RSV+HP, RSV+FBS and RSV+MP treated HEp-2 cells. Bar= 500 µm.

Supplementary Figure 3. (**A**) RSV preincubated with different biofluids and subsequently added to primary moDCs in serum-free conditions at MOI 1 for 48 h. CD86 was quantified by flow cytometry. (**B**) Dose response activation of moDCs by RSV preincubated with different amounts of BAL and added to the cells at MOI 1 for 48h in serum-free conditions. CD86 was quantified by flow cytometry. Non-parametric Kruskal-Wallis unpaired test followed by Dunn's post-test or Mann-Whitney test was used to compare the data. P-value: not significant (n.s) $P > 0.05$*. Statistics were calculated using GraphPad Prism 7 software.

Supplementary Figure 4. Different biofluids were diluted to a protein concentration of 0.3 mg/ml then ELISA was used for detecting RSV specific IgG antibodies.

Supplementary Figure 5. Gene list enrichment analysis of the total RSV corona profile in FBS and MP pre-treatment groups. The top five enriched terms are shown in each GO domain.

Supplementary Figure 6. Negatively stained TEM images of nanoparticles with 50 μM $A\beta_{42}$. White arrows indicate nanoparticles and black arrows indicate fibrillar structures, bar = 1 μm.

Figure 1.

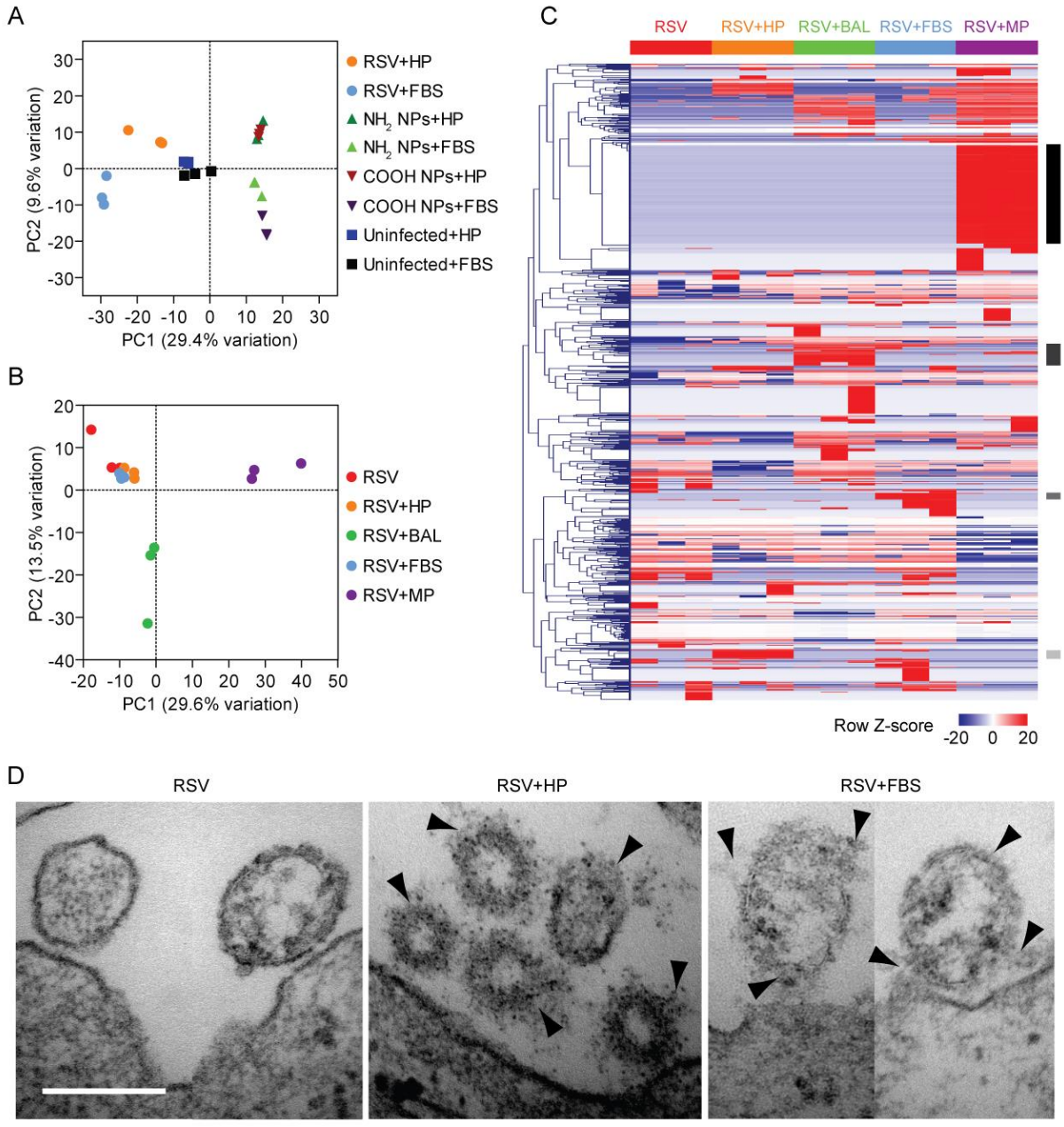

Figure 2.

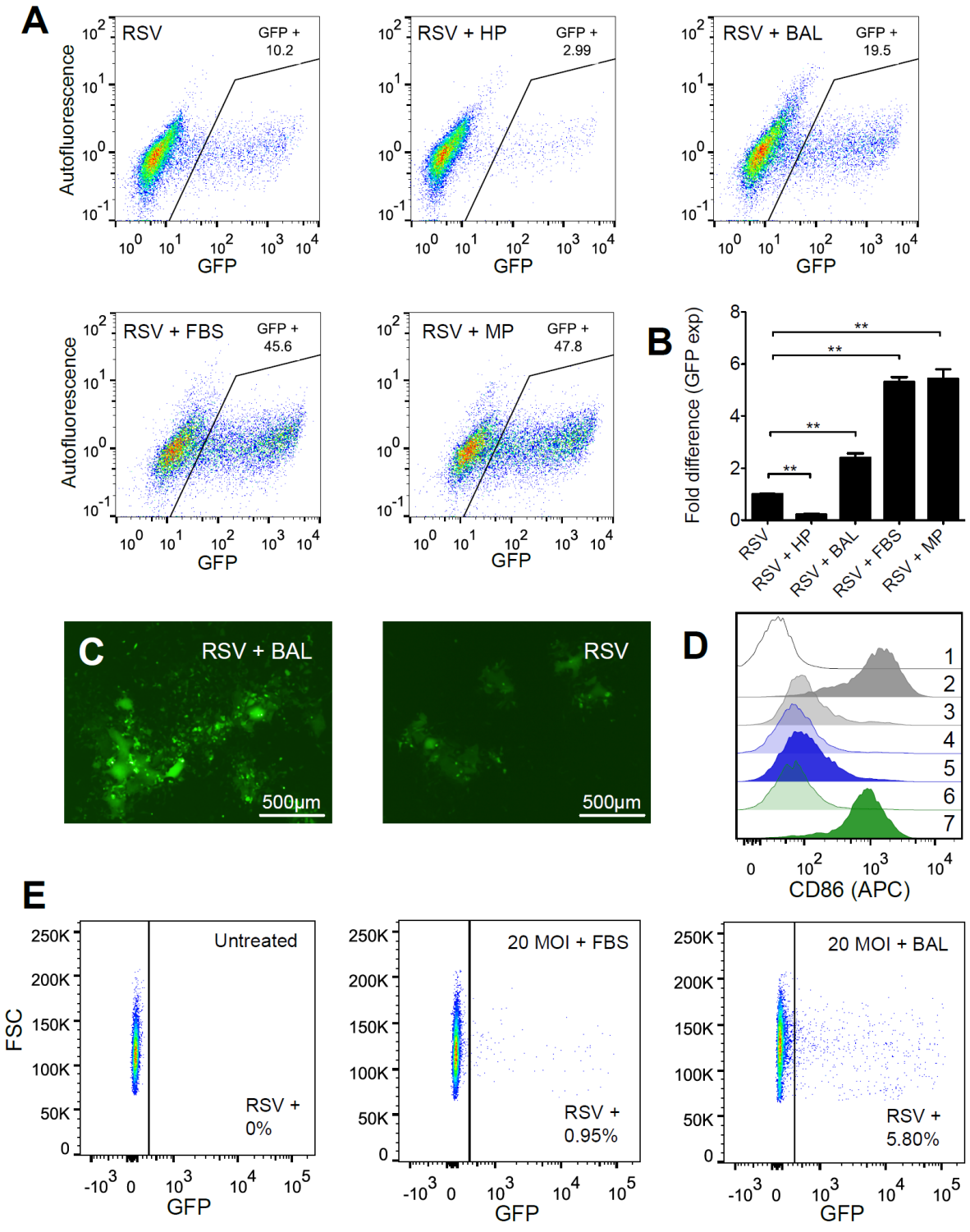

Figure 3.

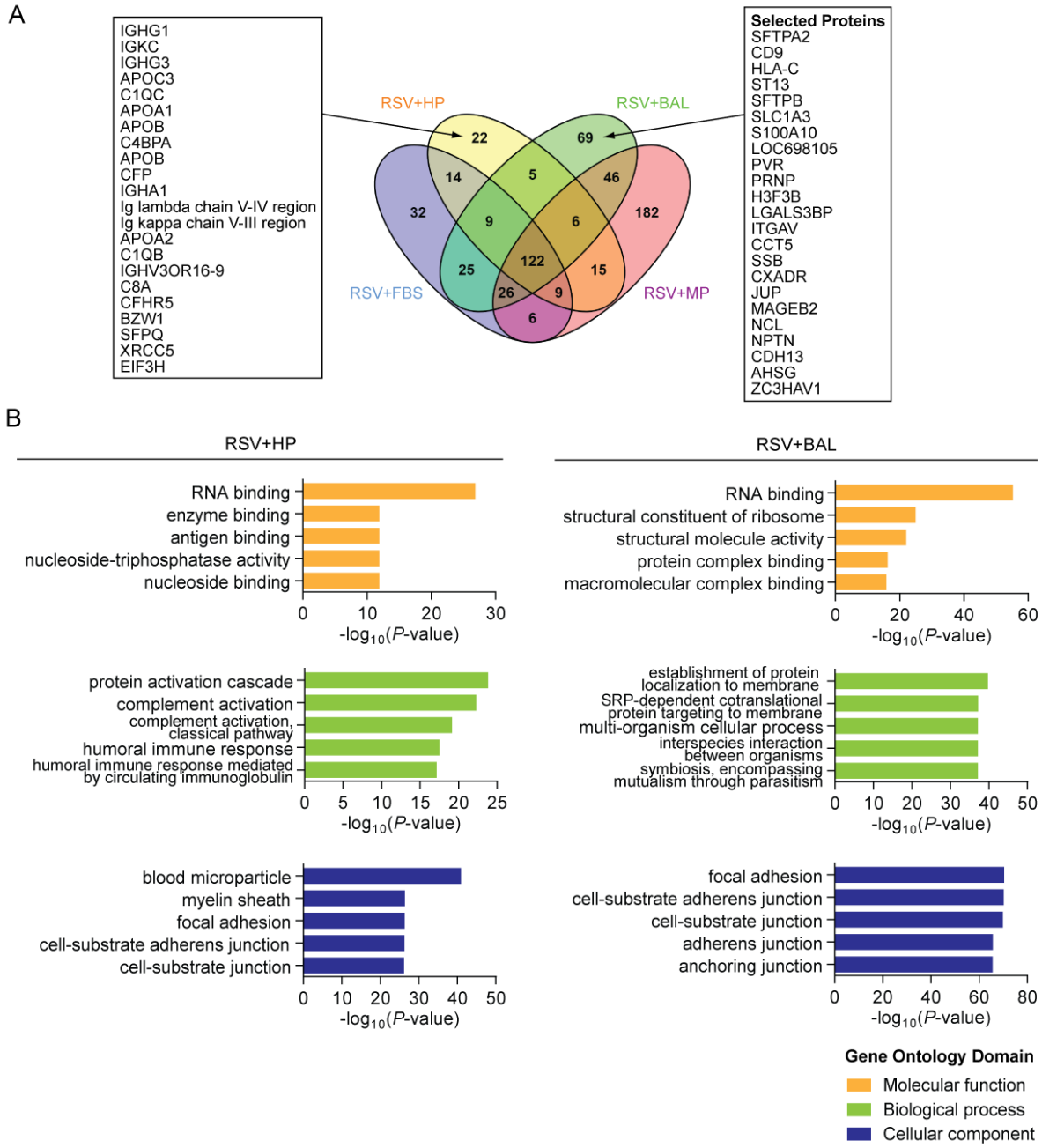

Figure 4.

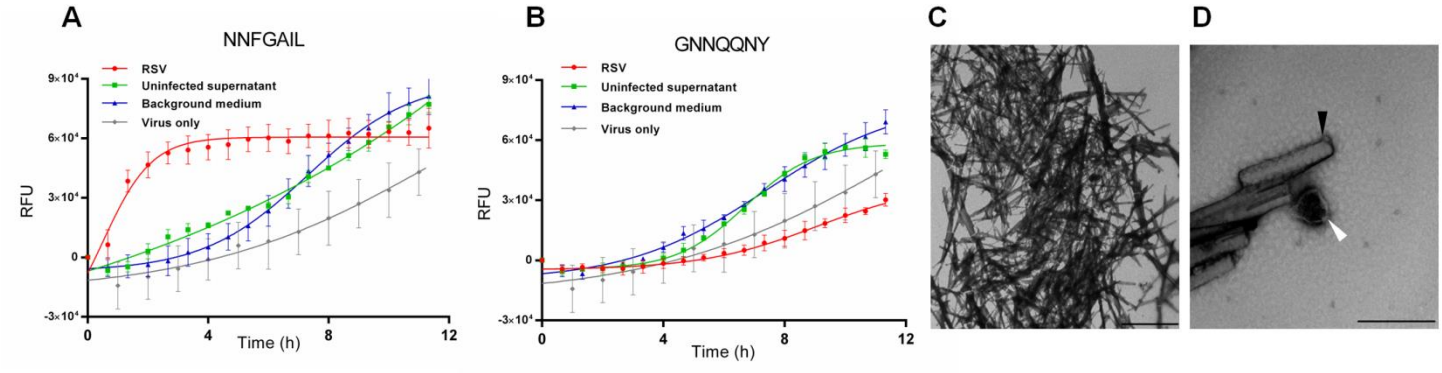

Figure 5.

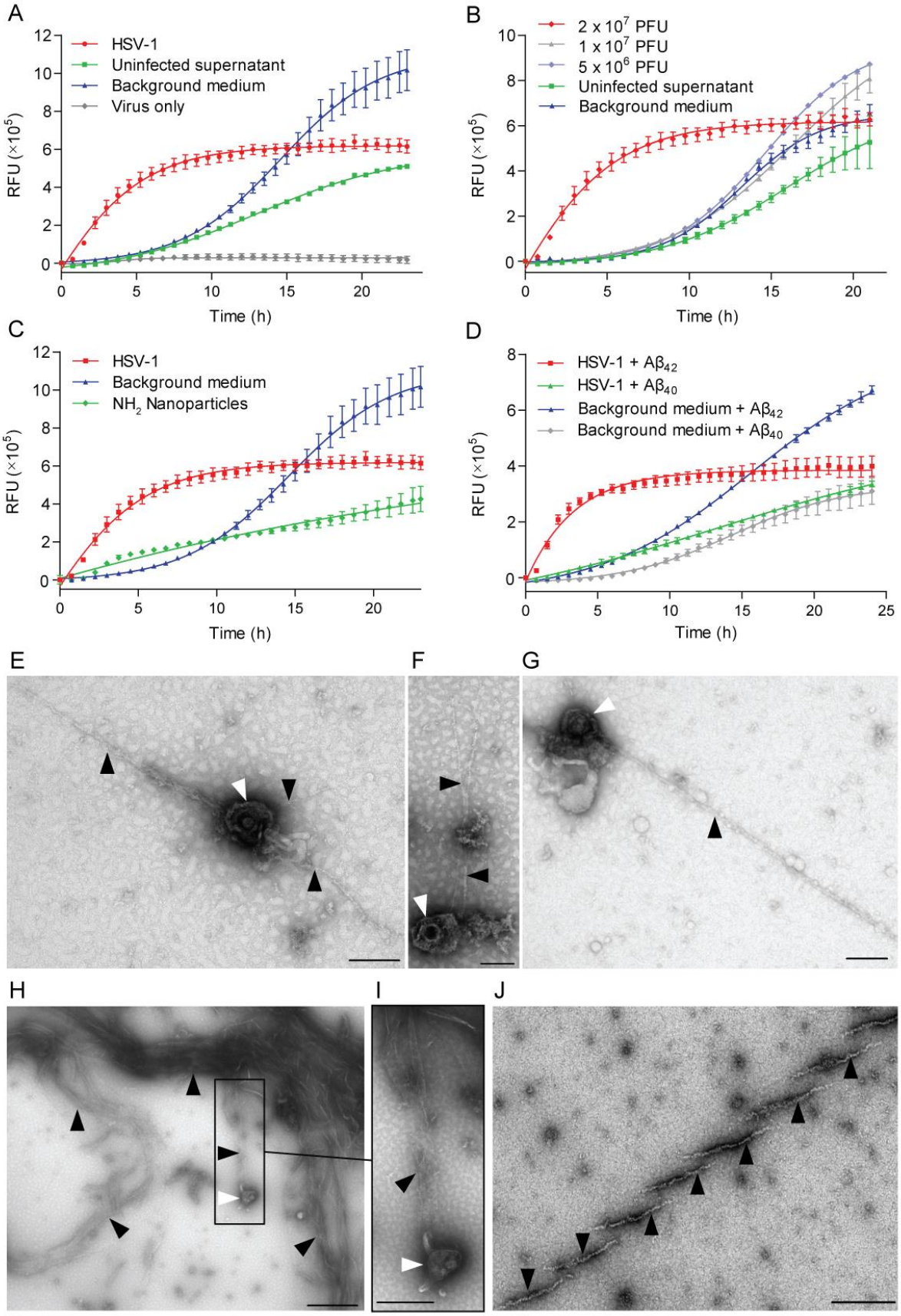

Figure 6.

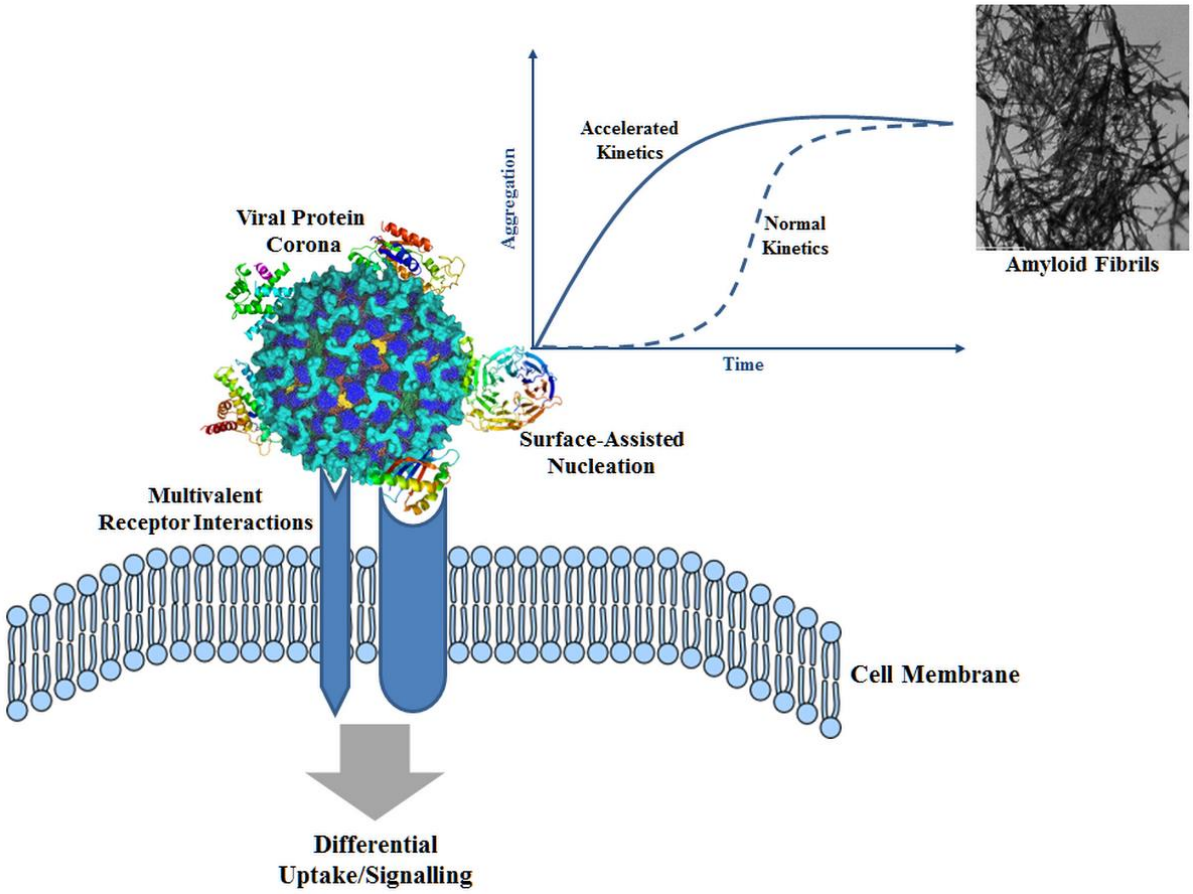

Supplementary Figure 1.

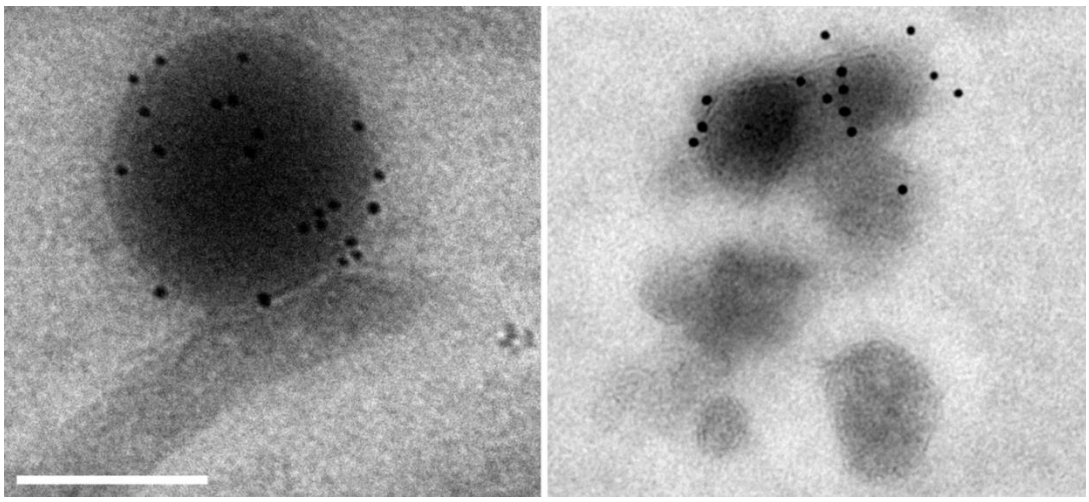

Supplementary Figure 2.

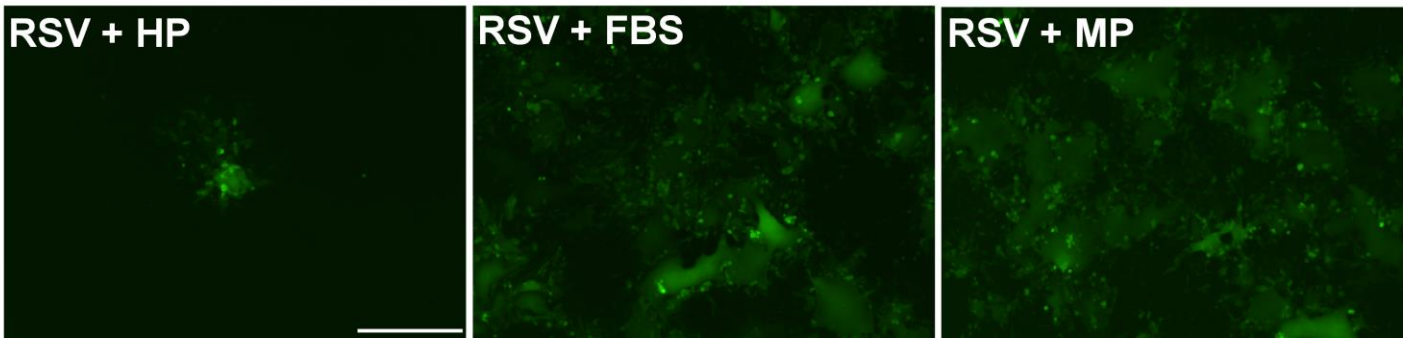

Supplementary Figure 3.

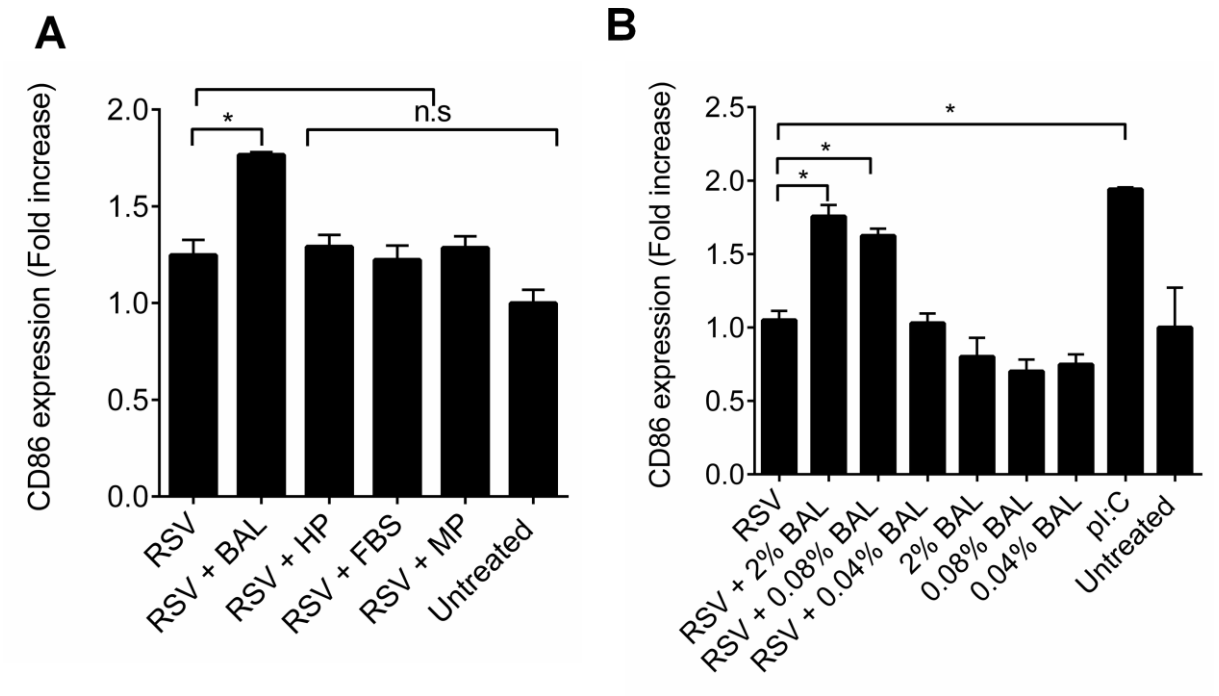

Supplementary Figure 4.

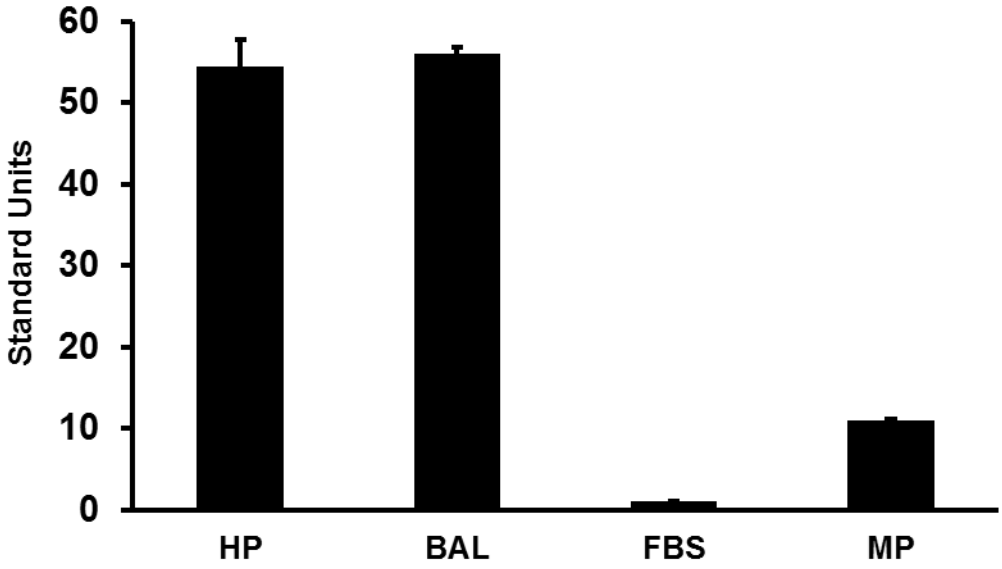

Supplementary Figure 5.

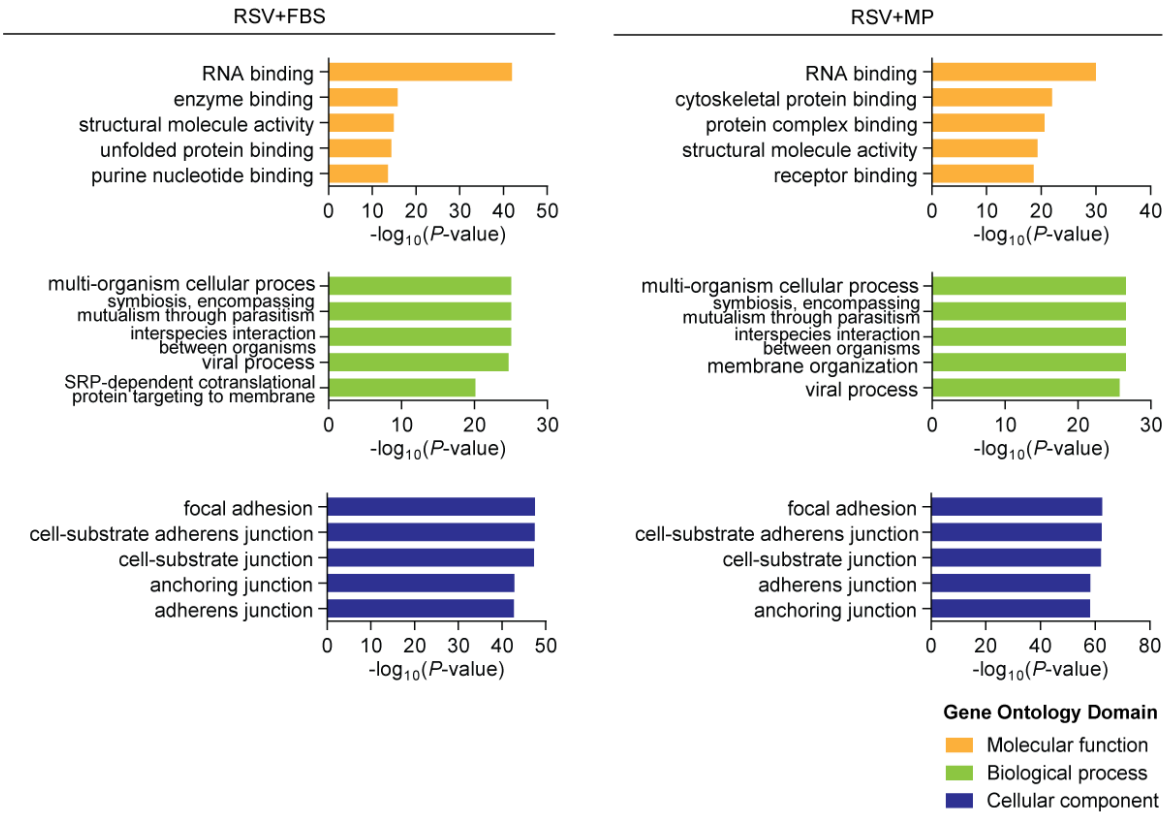

Supplementary Figure 6.